Topology of turbulent premixed and stratified LPG/air flames

Dhanalakshmi Sellan, Saravanan Balusamy *

Department of Mechanical and Aerospace Engineering, Indian Institute of Technology Hyderabad, Kandi, Sangareddy - 502285, Telangana State, India

A B S T R A C T

Premixed and stratified Liquefied Petroleum Gas (LPG)/air flames realized on a bluff body swirl-stabilized burner are studied in a confined environment. A laboratory-scale burner is designed in such a way that it can independently investigate the effects of mixture stratification, swirl number, swirl direction, and Reynolds number on a broad range of test conditions. A total of 80 different test cases are investigated, with four different swirl number combinations, two different swirl direction combinations, two velocity ratios, and five different mixture stratification ratios. The flame topology is investigated using the simultaneous acquisition of hydroxyl radical (OH*) and methylidyne radical (CH*) chemiluminescence and direct imaging. A series of premixed and stratified flame topologies are compared using mean Abel-deconvoluted chemiluminescence images and direct mean images. Premixed flames appear to be lifted V-flames influenced primarily by swirl number combinations rather than swirl direction or velocity ratio variations. For the same swirler combinations and velocity ratios, stratified flames are more compact than premixed flames, and higher stratified flames are similar in shape. A counter-rotating coaxial swirler arrangement is less likely to affect the flame structure than a change in swirl number. According to the study, the outer swirl angle determines the flame shape, whereas the inner swirl angle influences mixing, which aids in flame stabilization.

© 2021 Elsevier Masson SAS. All rights reserved.

1. Introduction

Modern gas turbine combustors are preferred to be operated in a fuel-lean premixed mode of combustion because it lowers the flame temperature and thus NOx emissions while maintaining combustion efficiency [1–6]. Stratified combustion, when compared to premixed combustion, can provide greater flame stability and ignitability in extremely lean fuel conditions [7–9]. Therefore, numerous studies using stratified burners have been carried out to understand the stratified mode of combustion better [10–15]. Several experiments have been carried out to determine the effect of stratification on flame speed, flammability limit, curvature, flame brush thickness, and flame surface density [16–20]. These studies found stratified flames advantageous over premixed flames in terms of enhanced flame speed, broader reaction zone, extended flammability limit, and resistance to flame stretching. There are two modes of stratified flames: back-supported and front-supported. When the flame propagates from stoichiometric mixture to lean mixture, the excess heat and radicals from the burned zone sustain the flame propagation through the leaner mixture, called 'back supported' [21]. On the contrary, favorable fresh mix-ture conditions supported flame propagation from lean mixture to stoichiometric mixture called 'front supported.' More research in rich stratified mixtures is needed to understand this scenario. The effect of stratification was also investigated by numerical simulations [22–25]. Masri [21], and Lipatnikov [26] have given a thorough review of experimental and numerical studies on the different modes of stratified combustion.

Swirlers are used in modern gas turbine combustors to stabilize the flame. The swirlers create recirculation to improve the mixing of hot gas with the fresh fuel-air mixture, which helps to stabilize the flame. Double swirler burners, which improve mixing and flame stability, have also gained attention recently [27]. The flow is featured with inner recirculation zone (IRZ) caused by vortex breakdown, outer recirculation zone (ORZ) caused by the sudden expansion of the flow from nozzle, stagnation points, inner shear layer (ISL), and outer shear layer (OSL) [14]. The IRZ formed due to interaction between the bluff body and inner flow, promotes the mixing of burned product with incoming stream [28–30]. All these features are affected by the swirl number and swirl directions along with the mixture stratification ratio [31–33]. The magnitude of the swirl significantly alters the flow/flame structure and the direction of the swirl considerably affects the flow features. De-geneve et al. [33] have conducted extended experiments to study the effect of co-rotating and counter rotating coaxial swirl flow on non-premixed flame. It is observed that counter swirl in the in-

---

* Corresponding author.
E-mail address: saravananb@mae.iith.ac.in (S. Balusamy).

ner flow weakens the central recirculation zone with higher swirl strength and makes flame elongated. In contrast to that low swirl at the outer strengthen the central recirculation zone and makes the flame compact.

Chemiluminescence in combustion is electromagnetic radiation released by the de-excitation of electronically excited species formed in the combustion reaction zone. The species such as CH^*, OH^*, C_2^* and CO_2^* are major species that are formed during the combustion of hydrocarbon fuels. Experimental studies have shown that the intensity of these species can be used to monitor heat release rate and fuel-air ratio [34,35]. Numerous studies have been conducted to identify the reaction zone in premixed flames [36–40] and a few in stratified flames using chemiluminescence measurements [41–43]. All of these studies show that quantitative measurements using the line-of-sight chemiluminescence emission are difficult and complex. In flames with independent strain rates, a direct correlation between intensity ratio (OH^*/CH^*) and equivalence ratio (ϕ) was obtained [35]. Whereas for strained flames, a direct correlation is difficult to achieve and appropriate calibration is required [43]. Despite being used to measure temperature and equivalence ratio, chemiluminescence can also be used to monitor instability by observing the heat release rate and macrostructure of the flames [14,44,45]. Furthermore, because the turbulent swirl flames are inherently three-dimensional, techniques such as the computed tomographic reconstruction of chemiluminescence are employed to study the structure of turbulent flames [45,46]. These recent studies show that computed tomography chemiluminescence can be used for instantaneous measurements with a large number of projections to achieve good spatial resolution or time-resolved measurements with a less number of projections that may fail to capture small details in turbulent flames [46]. For simplicity, in the present study, simultaneous measurements of OH^* and CH^* are used to observe the complex flame structures that vary depending on the operating and geometrical conditions.

In the interest of environmental protection and diversification of energy supplies for transportation, different types of fuels have been introduced as alternatives to traditional fossil fuels. Liquefied Petroleum Gas (LPG) is one of the best alternative fuels due to its availability, cost, and favorable combustion characteristics. As the LPG is low carbon fuel, it could be good intermediate fuel for energy and transportation sectors where there is no possibility of complete shifting from fossil fuel to zero-carbon sustainable energy. Several investigations have been conducted on the direct injection of LPG in gasoline engines [47–49]. LPG is also becoming a popular fuel for gas turbine engines due to its good combustion and low emission characteristics [50–52]. Therefore, a complete understanding of LPG combustion is required to implement it for practical application.

The present study investigates the topology of turbulent premixed and stratified LPG/air flames realized in an axisymmetric swirl-stabilized burner with a quartz tube enclosing the flame. The macrostructure of the flame is investigated using direct and OH^*/CH^* chemiluminescence imaging. One premixed ($\phi_g = 0.75$) and four stratified flames with different swirler combinations and velocity ratios are considered in the current experimental study. The stratified flames studied here are back-supported. The current paper is organized as follows. Begin with an experimental setup consisting of a stratified swirl-stabilized burner, operating conditions, and diagnostic techniques. The direct photographs and images of time-averaged Abel deconvoluted OH^* and CH^* chemiluminescence are shown and discussed in terms of how the flame responds to stratification, velocity ratio, swirl number, and swirl direction while maintaining a constant total thermal input.
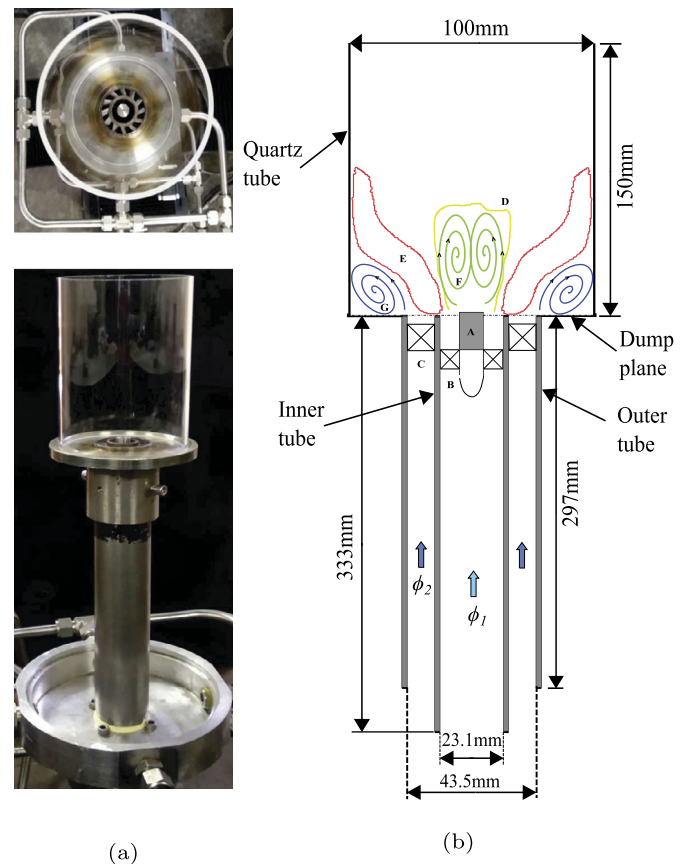

Fig. 1. Swirl-stabilized burner unit. (a) Top and side view of the burner, (b) Schematic diagram. (A) Bluff body; (B) Inner swirler; (C) Outer swirler; (D) Inner flame; (E) Outer flame; (F) Inner recirculation zone; (G) Outer recirculation zone; The equivalence ratios of the premixed mixture fed to the inner and outer annulus are specified as ϕ_1 and ϕ_2.

2. Experimental methodology

2.1. Burner

The turbulent premixed and stratified LPG/air flames are studied using a swirl-stabilized axisymmetric burner with a bluff body configuration. The burner was built to operate at a variety of stratification ratios, swirl numbers, and Reynolds numbers. The design philosophy of the burner with the co-flow air arrangement is found in [15]. In this work, the co-flow setup is replaced by a 150 mm long quartz tube with an inner diameter of 100 mm, which is used to stabilize the flame in a confined environment typical of realistic operation and to study the flame-wall interaction. The burner unit is depicted in Fig. 1, which consists primarily of two annuli formed by inner and outer tubes, two axial swirlers known as the inner and outer swirlers, a bluff body, and a quartz tube. A 333 mm long inner tube houses a bluff body with a diameter of 12 mm and an axial swirler with an outer diameter of 23.1 mm. To generate an inner flame above the bluff body, a premixed fuel-air mixture with an equivalence ratio ϕ_1 is supplied through the inner tube. The inner flame which is stabilized by the bluff body and inner swirler plays a crucial role in the stabilization of the outer flame and the inner flame is maintained to be richer than the outer flame at stratified conditions. The outer annulus is formed by a 297 mm long outer tube with an inner diameter of 43.5 mm, through which another premixed fuel-air mixture of equivalence ratio ϕ_2 is supplied to generate the outer flame, as depicted in Fig. 1(b). Inner and outer swirlers contribute to the formation of an inner recirculation zone above the bluff body, as

Table 1
Details of 3D printed swirlers.

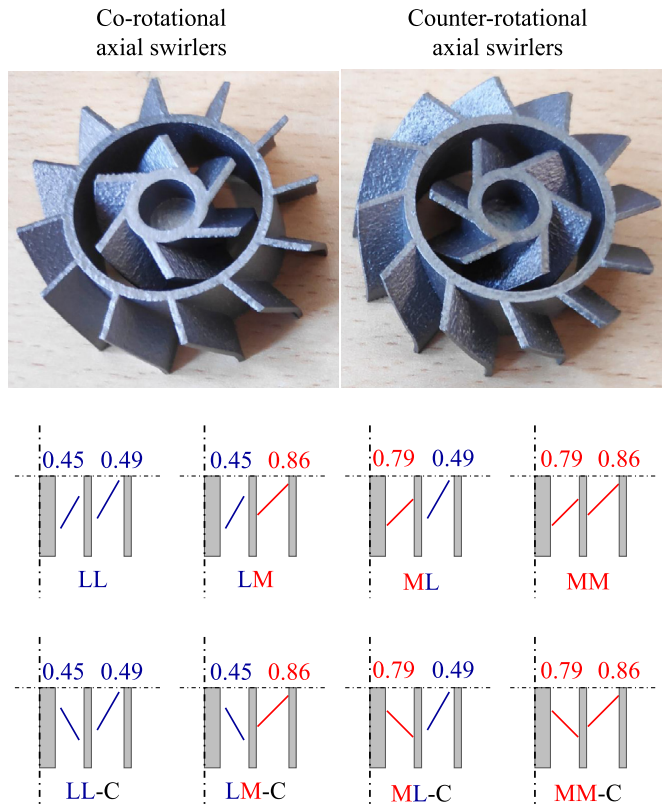| Swirler location	Swirl angle	No. of Vanes	Swirl number (S)
Inner annulus	30°	6	0.45
	−30°	6	0.45
	45°	6	0.79
	−45°	6	0.79
Outer annulus	30°	12	0.49
	45°	12	0.86

Fig. 2. Top row shows 3D printed coaxial swirlers with co-rotating and counter-rotating (C) flow configurations. Middle and bottom row show schematic diagrams of swirler combinations. The numbers above the burner exit indicate the geometrical swirl number in each annulus.

well as an outer recirculation zone between the outer flame and the quartz tube near the burner exit.

The effect of swirl number and swirl direction on flame and flow topology is investigated using the six different axial swirlers listed in Table 1. These swirlers are made with metal 3D printing and have a low (L, $\theta = 30°$) or medium (M, $\theta = 45°$) swirl angle with a co-rotating ($\theta > 0$) or counter-rotating (C, $\theta < 0$) swirl flow direction. The swirler vane thickness is kept as 1 mm. The swirl number is defined as the tangential to axial momentum ratio estimated from the geometry of swirler [53]. Fig. 2 shows an example of inner and outer swirlers in co-rotating and counter-rotating flow configurations. Two sets of co-rotating swirlers are used in the outer annulus, while two sets of co-rotating and two sets of counter-rotating (C) swirlers are used in the inner annulus. As a result, eight different swirl flow combinations are realized by interchanging co-rotating and counter-rotating swirlers with the low (L) or medium (M) swirl numbers as depicted in Fig. 2.

The flow configuration schematic for the experimental setup is depicted in Fig. 3. The mass flow rates of LPG (60% of Propane and 40% of Butane) and compressed air are metered separately by mass flow controllers (MFC - Alicat MCR-D Series) with an uncer-

tainty of ±1 of full scale. The regulated flows of LPG and air are fully premixed in a mixing chamber before entering the burner. An extraction system is used to transport the burned products to the atmosphere.

2.2. Operating conditions

The effect of mixture stratification, swirl direction, swirl strength, and shear strength between streams is investigated in this work using a detailed test matrix, which is shown in Table 2. The total thermal power input ($\dot{Q}_{thermal}$ = 25 kW) is kept the same for all the cases. The velocity ratio (VR) is defined as the ratio of the outer bulk velocity (U_2) to the inner bulk velocity (U_1), and varied from 2 and 3 to study the effect of shear strength between different streams. The stratification ratio (SR) is the ratio of the inner equivalence ratio (ϕ_1) to the outer equivalence ratio (ϕ_2), where SR1 denotes premixed flames and SR2 to SR5 denote stratified flames. Table 2 also shows the Reynolds number (Re = $\rho U d / \mu$) derived from the bulk velocity (U) and the exit geometry (hydraulic diameter, d).

2.3. Chemiluminescence imaging

Chemiluminescence imaging is a non-intrusive optical diagnostic tool that can be used to study intermediate free radicals in the reaction zone [54]. The radicals OH* and CH* are perhaps the most common species formed during the combustion of hydrocarbon fuels and literature shows that the intensity of chemiluminescence from these radicals might be a good indicator of heat release rate [35,55,56]. In the present study, the intensities of OH* and CH* chemiluminescence are simultaneously recorded. The experimental configuration of chemiluminescence imaging is illustrated in Fig. 4. The OH* and CH* signals are collected using two Intensified Charge-Coupled Device (ICCD) cameras (PIMAX-4, Princeton Instrument) with the pixel resolution of 1024 × 1024 pixels. Cameras are equipped with a 105 mm Nikon UV objective lens (f/5.6) and band-pass filters. The intensity of OH* is acquired using a 25 mm color glass UV pass filter (FGUV11, Thorlabs) with a wavelength range of 275 - 375 nm, and the intensity of CH* is collected using a 430 ± 2 nm band-pass filter (FB430-10, Thorlabs). The flame structure is derived from an average of 500 instantaneous images taken at 10 frames per second and with a field of view of 130 mm × 130 mm. The camera captures each image with a gate width of 5 ms. The cameras are synchronized for simultaneous OH* and CH* measurements with the SuperSYNCHRO timing generator, which controls the synchronization timing between the two cameras.

The collected line-of-sight chemiluminescence data are needed to be converted into field information. The Abel transform is a sophisticated analytical method for deconvoluting data to extract spatially resolved information from temporally averaged line-of-sight optical measurements acquired from an axisymmetric domain using non-intrusive diagnostic techniques. Assuming symmetry of the averaged chemiluminescence data, Abel-deconvolution is applied here to get the information at the mid-plane of the burner axis. The field distribution $F(r_j)$ is obtained by deconvoluting the projection data $P(r_j)$ at spacing Δr by using the equation given below [57]

$$F(r_j) = \frac{1}{\Delta r} \sum_{j=0}^{\infty} D_{ij} P(r_j)$$

where $r_i = i \Delta r$ is the distance from the center of the object. The linear co-efficient D_{ij} is differential operator on the $P(r_j)$ which
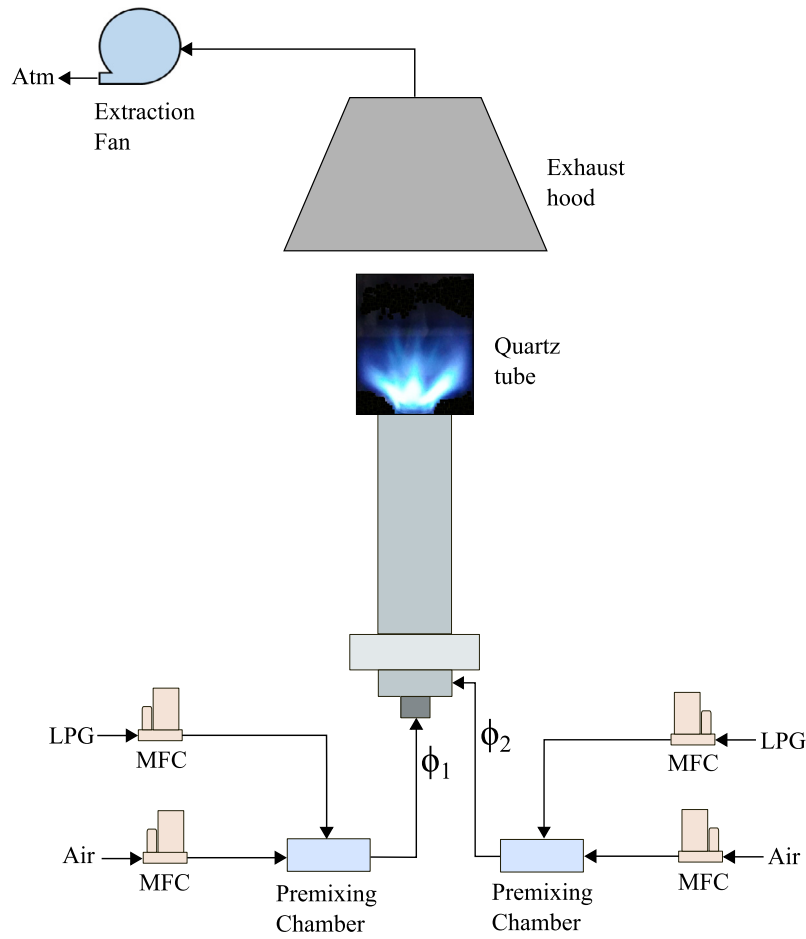
Fig. 3. Schematic diagram of the experimental setup.

Table 2
The operating conditions of the swirl-stabilized burner. In all cases, $\dot{Q}_{thermal}$ = 25 kW.

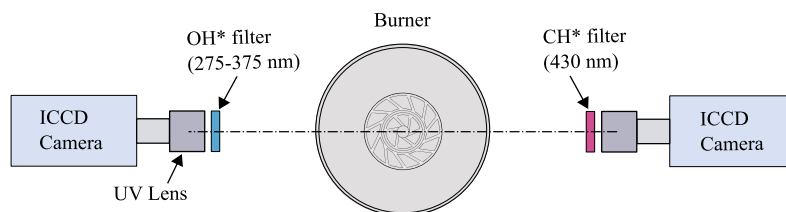| Velocity ratio (VR) (U_2/U_1)	Stratification ratio (SR) (ϕ_1/ϕ_2)	Case number	Inner stream			Outer stream		
			Equivalence ratio (ϕ_1)	Bulk velocity (U_1) in m/s	Reynolds number (Re_1)	Equivalence ratio (ϕ_2)	Bulk velocity (U_2) in m/s	Reynolds number (Re_2)
2	1	c1	0.75	5.69	4304	0.75	11.33	10420
	2	c2	1.00	7.32	5646	0.50	14.57	13133
	3	c3	1.20	7.97	6234	0.40	16.05	14356
	4	c4	1.40	8.21	6522	0.35	16.26	14477
	5	c5	1.60	8.08	6507	0.32	11.98	14330
3	1	c6	0.75	4.03	3044	0.75	11.98	11017
	2	c7	1.00	5.34	4113	0.50	16.10	14519
	3	c8	1.20	6.13	4795	0.40	18.17	16253
	4	c9	1.40	6.40	5086	0.35	19.02	16941
	5	c10	1.60	6.42	5174	0.32	19.28	17130

Fig. 4. Simultaneous OH*/CH* imaging setup.
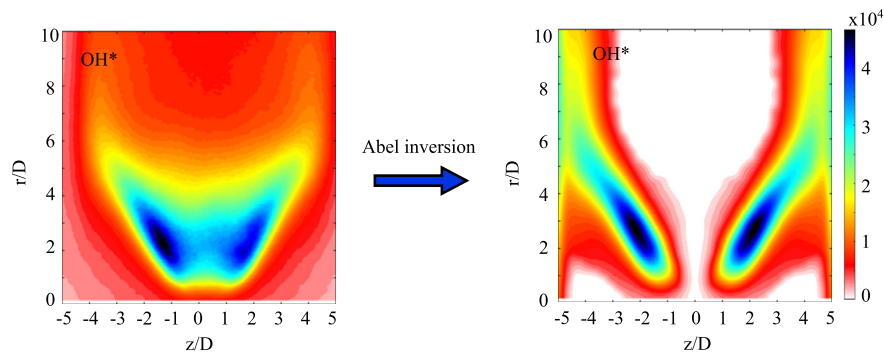
Fig. 5. Line-of-sight data (left) is Abel-deconvoluted into time-averaged field data (right). (For interpretation of the colors in the figure(s), the reader is referred to the web version of this article.)
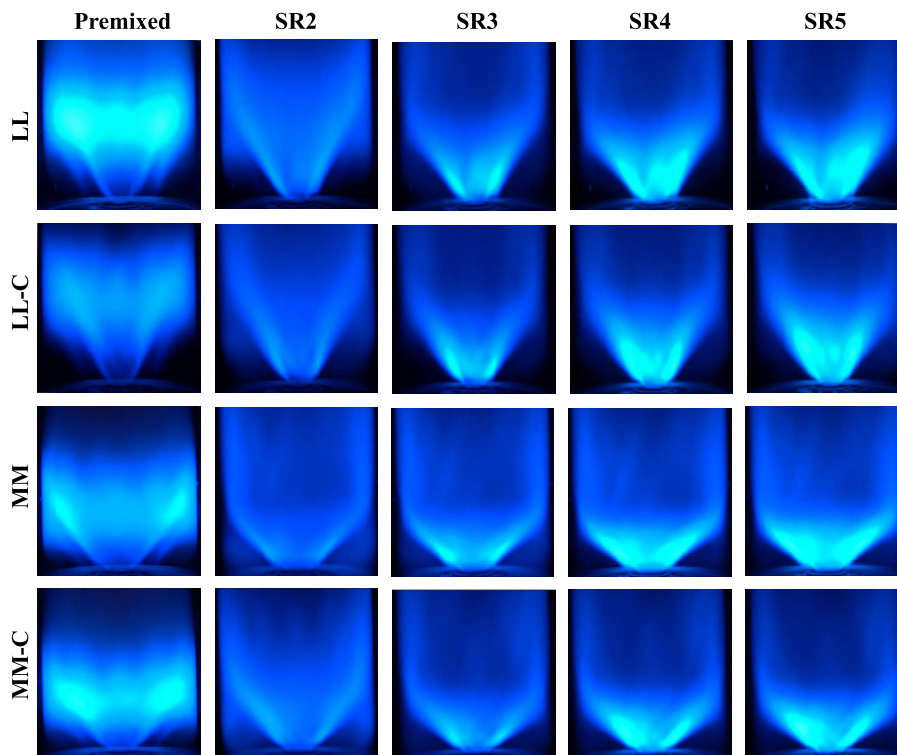

Fig. 6. Time-averaged direct images of premixed and stratified flames (SR2 to SR5) for VR2 at co-rotating and counter-rotating (C) swirl combinations of LL and MM.

localized in the region of r_j. The MATLAB code based on this algorithm is used to obtain the planar data from the line-of-sight information. Figure 5 illustrates Abel-deconvoluted data plotted from the line-of-sight data which is shown on left side.

3. Results and discussion

Direct flame imaging and chemiluminescence imaging are used in 80 different cases to investigate premixed and stratified flame topology and flame-wall interactions. This section discusses the experimental results to determine the effect of stratification, velocity ratio, swirl number, and swirl direction on the flame structure.

3.1. Direct imaging of premixed and stratified flames

For reacting flows, direct images are captured first to obtain a qualitative understanding of the flame topology. The natural luminescence of the flames was taken at 1000 frames per second using a DSLR camera (Sony Cybershot DSC-RX10M2) without any filters. For all the cases examined here, the camera settings are main-

tained constant, and the time-averaged photographs are generated with MATLAB code. Fig. 6 shows the direct images of the premixed flames (first column) and stratified flames with LL and MM swirler combinations. As the swirl numbers (LL to MM) increase in premixed flame cases, the peak luminosity of the flame moves closer to the burner exit in both co-rotating and counter-rotating swirl configurations due to better mixing between hot burned products with incoming fresh mixture, enhancing the flame stabilization. There is not much of a distinction between the co-rotating and counter-rotating flame structures based on direct imaging.

The time-averaged direct images of all the cases are shown in the supplementary material (Fig. S1). Each has a distinct flame shape, though higher stratified (SR3 to SR5) flames are similar for a given swirler combination and velocity ratio when compared to premixed and SR2 flames. All premixed flames are elevated from the combustor exit and stabilized on the quartz tube wall, regardless of swirl number, swirl direction, or velocity ratio. When we switch from premixed to stratified (SR2) with the same global equivalence ratio (ϕ_g = 0.75), the flame appears with less luminosity due to the lean outer condition. The flames become more
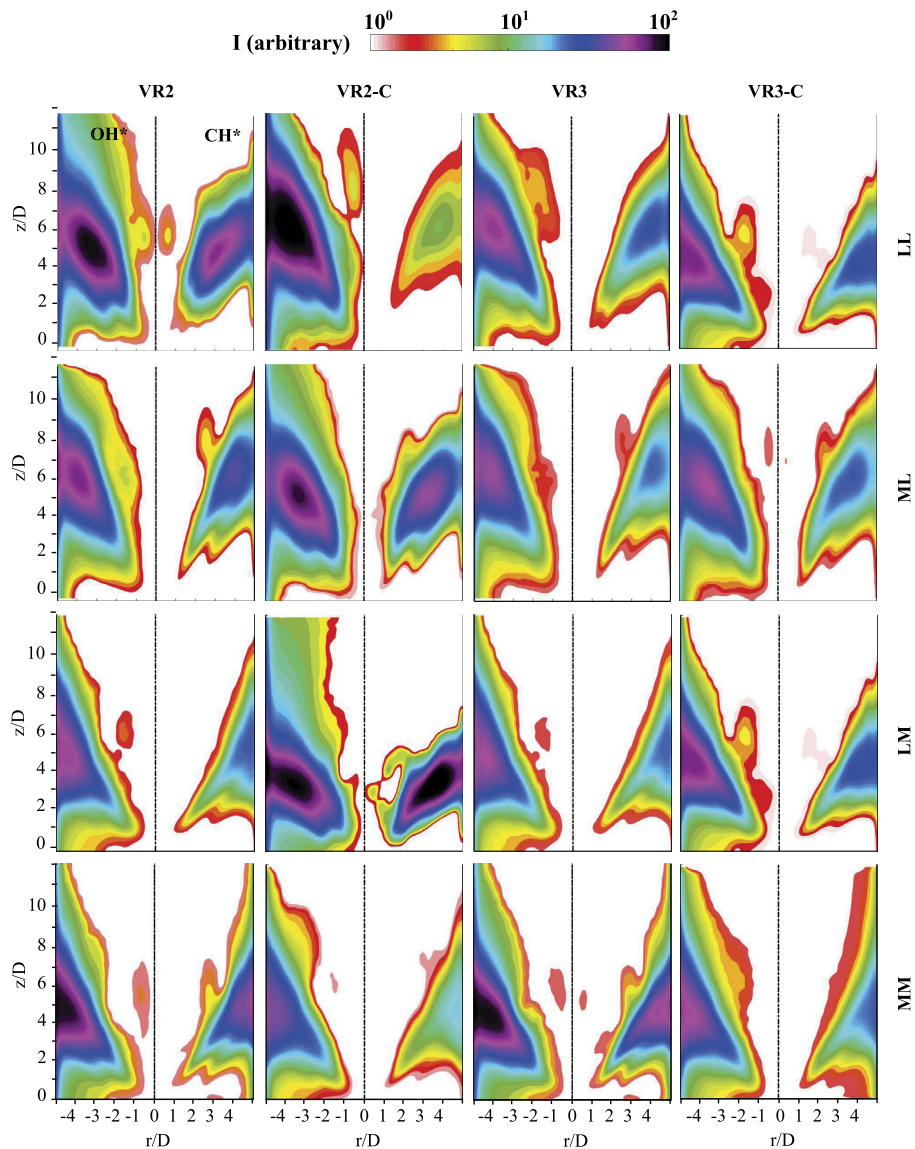
Fig. 7. Abel deconvoluted mean chemiluminescence intensity of OH* (r/D<0) and CH* (r/D>0) for premixed flames (SR1) with various swirl configurations (row-wise) and velocity ratios (column-wise). The color map is shown in logarithmic-scale.

luminous and compact as the stratification degree increases with the global equivalence ratio. All stratified flames are attached with the burner exit as the flame speed increases in stratified conditions due to the back support from the inner rich mixture [10]. Furthermore, because stratified flames are more compact, the heat transfer to the wall could reduce compared to premixed conditions.

3.2. Topology of premixed flames ($\phi_g = 0.75$)

The topology of premixed flames under various operating conditions is investigated using simultaneous imaging of OH* and CH*. The acquired images are Abel-inverted to reveal the OH* and CH* distribution at the mid-plane of the burner [15]. Fig. 7 shows chemiluminescence images of premixed flames with different swirler combinations and velocity ratios. Assuming symmetry, OH* intensity is shown in the left half (r/D<0), and CH* is shown in the right half (r/D>0). Owing to its longer life span, OH* appears to be spread out more than CH* in all these intensity plots. The flame structure for the LL and ML swirl combinations appears to be identical, as does the flame structure for the LM and MM swirl combinations. The structure of the flame is ultimately determined by the outer swirl number. As seen in the direct imaging, the flames appear elongated axially for LL swirl combinations, and this is also true for ML swirl combinations. The MM and LM swirl combinations, on the other hand, result in a broader flame structure.

When premixed flames from co-rotating and counter-rotating swirl conditions are compared, counter-rotating flames of all swirl combinations except MM swirlers have higher OH* intensity. The turbulent level is higher in counter-rotating swirler combinations of LL, ML, and LM, which improves fuel-air mixing and increases radical formation due to improved combustion. However, counter axial rotation, combined with higher swirl strength, generates more turbulence in the MM swirl combination, resulting in a dominant turbulent time scale over the chemical time scale. Since the OH* and CH* chemiluminescence emission indicates the location of the reaction zone [35], it is seen that all premixed flames are detached from the combustor exit and stabilized at the quartz tube boundary further downstream. As a result, all of the premixed flames appear to be lifted V-flames, possibly due to the flame speed being lower than the total flow bulk velocity [10].
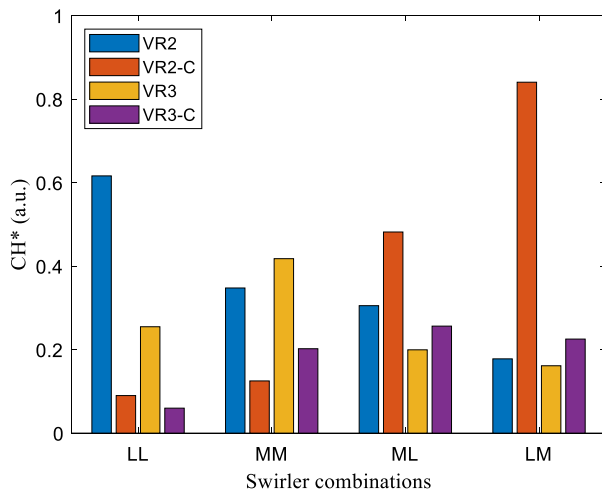
Fig. 8. Cumulative CH* intensity for various swirler combinations of premixed flames.

Since the flames stabilize at the quartz tube wall, there is more contact between the flame and the wall. Consequently, there is a greater chance of heat transfer to the quartz tube wall, which is undesirable in practical applications.

Fig. 8 depicts the cumulative CH* emission, which is the integration of intensities from the mean image of each condition, to help understand the effect of velocity ratio on premixed flames. Except for MM swirl combinations, the intensity of CH* is higher in velocity ratio VR2 than in VR3 for each swirler combination, whether co-rotating and counter-rotating. In the MM swirl combination, there is a strong interaction between the inner and outer streams, which could enhance radical and heat diffusion from the inner rich to the outer lean stream. The LM with counter-rotational flow produces more CH* than all other conditions at velocity ratio VR2 conditions, regardless of swirl number or swirl direction.

3.3. Stratified flame SR2 with ϕ_g = 0.75

Fig. 9 shows the Abel deconvoluted mean chemiluminescence intensity of OH* and CH* for stratified flames (SR2) with the same premixed flame global equivalence ratio (ϕ_g = 0.75) for all operating conditions. The flame structure for the LL and ML swirl combinations appears identical, as does the flame structure for the LM and MM swirl combinations. The outer swirl number has more influence on the structure of the flame. Stratified conditions have a very different flame structure than premixed conditions. The reaction zone moved upstream due to the increased flame speed supported by the inner stoichiometric stream. However, the intensity has been dropped at least an order of magnitude compared to equivalent premixed flames, which shows that the overall reaction rate dropped significantly in the outer stream. When the inner swirl level is increased from low to moderate, the flame shape did not change, and it appears to be lifted V-flames. When the outer swirl is increased from low to moderate while the inner swirl remains low, the flame shape changes dramatically, resembling a lifted U-flame. Also, a similar trend holds for flames stabilized with moderate inner and outer swirls. The LM swirler with the co-rotating swirl configuration of VR2 has the most compact flame among the cases due to better back support from the inner stream to the outer lean stream.

The cumulative CH* intensity profiles of stratified flames (SR2) at all velocity ratios and swirler combinations are presented in Fig. 10. Both LM and ML swirler combinations show one trend with the switching of co-rotating and counter rotations, which is opposite to the LL and MM combinations. For example, the cumu-

lative intensity along the axial direction either the same or higher than the co-rotating configuration for LM swirlers. However, a significant drop in the intensity is observed for the LL with counter-rotation as compared to the co-rotating configuration. Nonetheless, the cumulative intensity along the axial direction decreased significantly with a higher velocity ratio (VR3) when compared to VR2 for all swirler combinations. This effect could be attributed to local quenching caused by higher turbulence levels.

3.4. Higher stratified flames with $\phi_g > 0.75$

Higher mixture stratification cases (SR3, SR4, and SR5) with corresponding global equivalence ratios of 0.8, 0.875, and 0.96 are discussed in this section. Fig. 11 shows the Abel deconvoluted mean OH* and CH* images of velocity ratio VR2, with all the swirler combinations for higher SR cases. Based on OH* and CH* intensity, in all highly stratified flames, the combustion zone is further moved upstream compared to premixed and SR2 flames, which is mainly due to flame speed enhancement by the back support from the rich inner mixture to leaner outer mixture in the form of heat and chemical radicals. Also, in some regions, the local equivalence ratio will reach closer to the stoichiometric due to the rigorous mixing of inner and outer streams. This qualitative investigation demonstrates that as the stratification ratio increases, there may be more heat release, which is not limited to the LM swirl combination. Even though the global equivalence ratios differ, the flame morphologies for all three stratified conditions (SR3, SR4, and SR5) remain identical under the same swirl condition and direction. As seen in the direct images (Fig. 6), the swirler combinations have the most influence on the flame shape, while stratification has very little. Because the flame shape is ultimately determined by the outer stream condition, the flame shapes of the LL and ML, as well as the LM and MM, are identical. The flame appears elongated in LL and ML swirl combinations but wider in MM and LM swirl combinations due to the higher outer swirl number.

When the effect of swirl direction is considered, flame behavior varies depending on the swirler combinations studied here. In the LL swirl combination, the counter-rotating swirl flame spreads slightly wider than the co-rotating swirl flame and prefers to move to the wall. This is also true for the LM swirl combination. In the case of the MM swirl combination, however, the flame becomes more compact and short in counter-rotating swirl conditions than in co-rotating swirl conditions, resulting in less contact with the wall and thus less heat transfer to the wall.

Fig. 12 shows the chemiluminescence intensity of highly stratified flames at velocity ratio VR3 for all swirler combinations with co-rotating and counter-rotating conditions. At VR3, where the outer bulk velocity is three times that of the inner bulk velocity, the flame becomes compact and emits less chemiluminescence than at VR2, regardless of swirler combinations or directions (Fig. S2 in the supplementary material). This is because VR3 has a higher mass flow of a leaner outer flame than VR2. The topology of the flame, however, is unaffected by stratification under any swirler combinations. The counter-rotating flows, as seen in VR2, also influence the flame structure in VR3. Among the stratified flames, SR4 has the most compact flame shape at any swirler combination or velocity ratio, indicating that this stratification ratio is optimal.

The cumulative CH* intensity profiles of stratified flames SR4 for various conditions are depicted in Fig. 13. The top row compares swirler combinations for VR2, while the bottom row compares swirler combinations for VR3. Since the topology of all stratified flames is identical, only SR4 is presented here to discuss the effect of swirl and velocity ratio. For LM and ML swirler combinations, both co-rotating and counter-rotating flames have the same intensity ranges, as does the velocity ratio VR3. In comparison, at
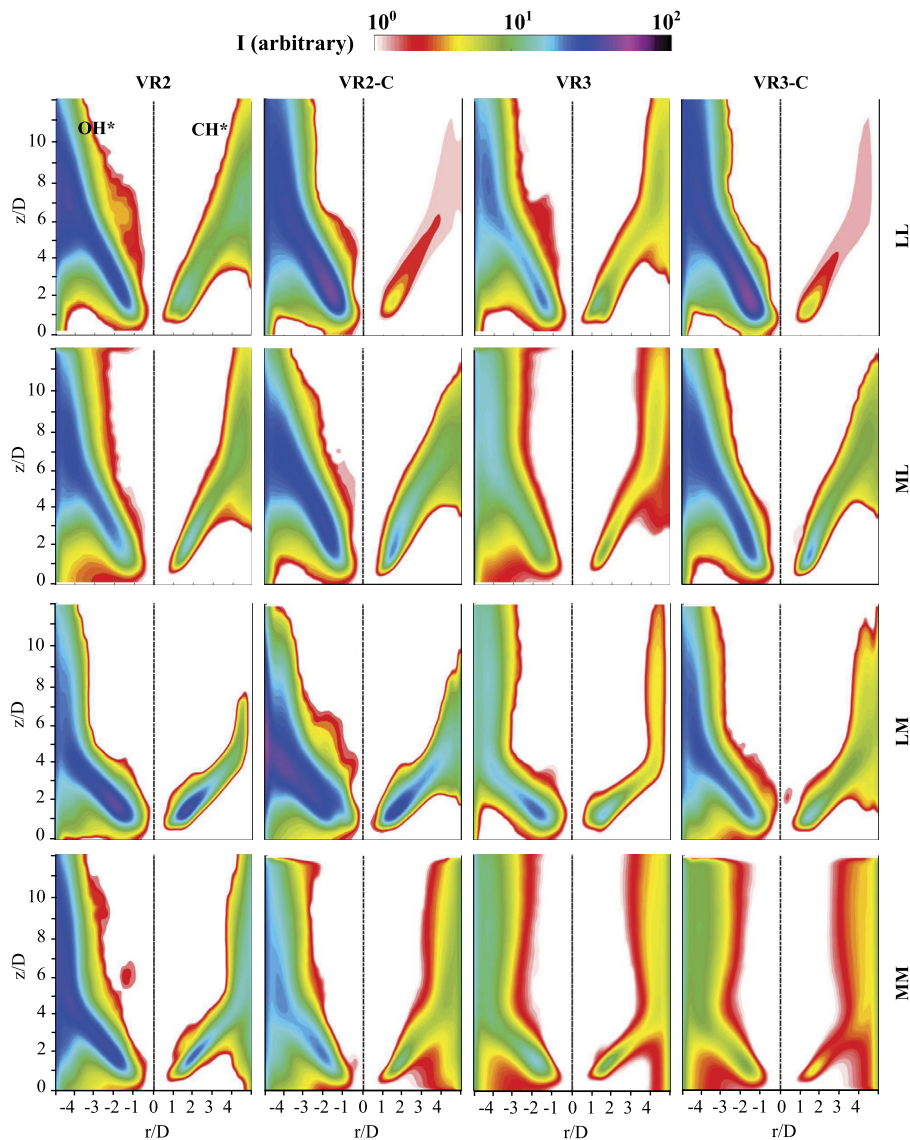
Fig. 9. Abel deconvoluted mean chemiluminescence intensity of OH* (r/D<0) and CH* (r/D>0) for stratified flames (SR2) with various swirl configurations (row-wise) and velocity ratios (column-wise). The color map is shown in logarithmic-scale.

any velocity ratio, having a similar swirl number in both the inner and outer flow greatly affects the flame structure. The intensity of the CH* chemiluminescence level decreases as the condition is changed from VR2 to VR3. The swirl number, swirl direction, and velocity ratio all influence the flame shape. As a result, while stratification does not affect the morphology of highly stratified flames, swirl number, swirl direction, and velocity ratio does (Figs. S3 and S4 in the supplementary material).

4. Conclusions

Experiments are conducted on premixed and stratified LPG/air flames ranging from homogeneously premixed (SR1) to highly stratified (SR5), with changes in velocity ratios (VR2, VR3), swirler combinations (LL, ML, LM, and MM), and swirl directions (co-rotating and counter-rotating). Simultaneous measurements of OH* and CH* reveal the flame structures for various operating and geometrical conditions. Direct imaging is also used to compare the structure of the turbulent premixed and stratified flames. The following conclusions can be drawn from the aforementioned experimental studies:

- Photographic images are used to compare the premixed and stratified flames, revealing that all premixed flames tend to elevate from the burner exit and stabilize on the quartz tube wall. In contrast, all stratified flames are compact and have less contact with the wall.

- In comparison to premixed flame, stratified flame with the same global equivalence ratio (ϕ_g = 0.75) shows a significant difference in structure and intensity, which is captured by direct and chemiluminescence imaging. When the condition is changed from a velocity ratio of 2 to 3, the flame structure does not change significantly, but the intensity of the combustion is reduced due to the dominance of turbulence interaction with flame structure. Cumulative CH* intensity profiles show that counter-rotating coaxial swirl flames have less CH* intensity than co-rotating swirl flames at the same medium (MM) and low (LL) swirler combinations.

- The structures of the highly stratified flames (SR3, SR4, and SR5) are identical, as demonstrated by direct and chemiluminescence imaging. It shows that stratification provides greater resistance to flame stretch. Even though the outer flame is lean, it is supported by the rich inner flame through back-
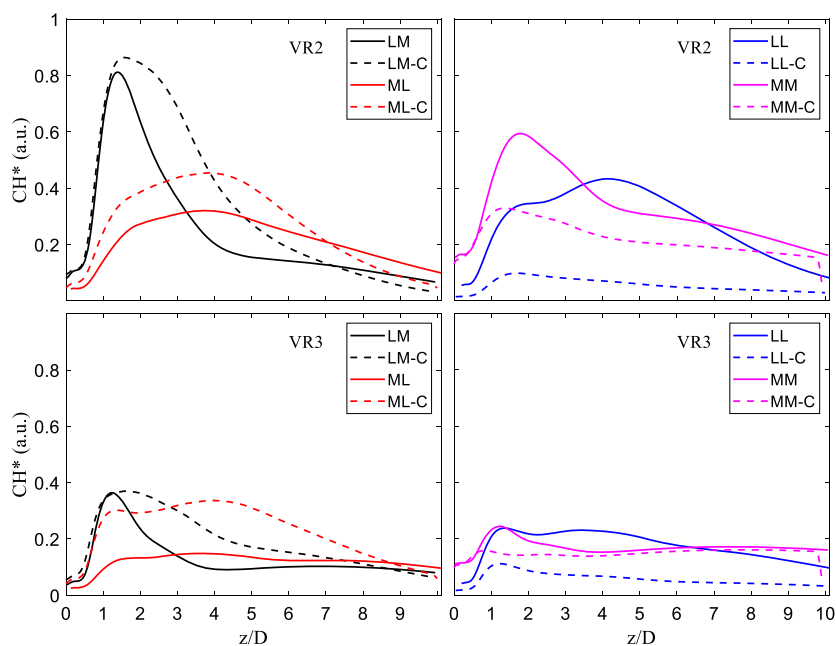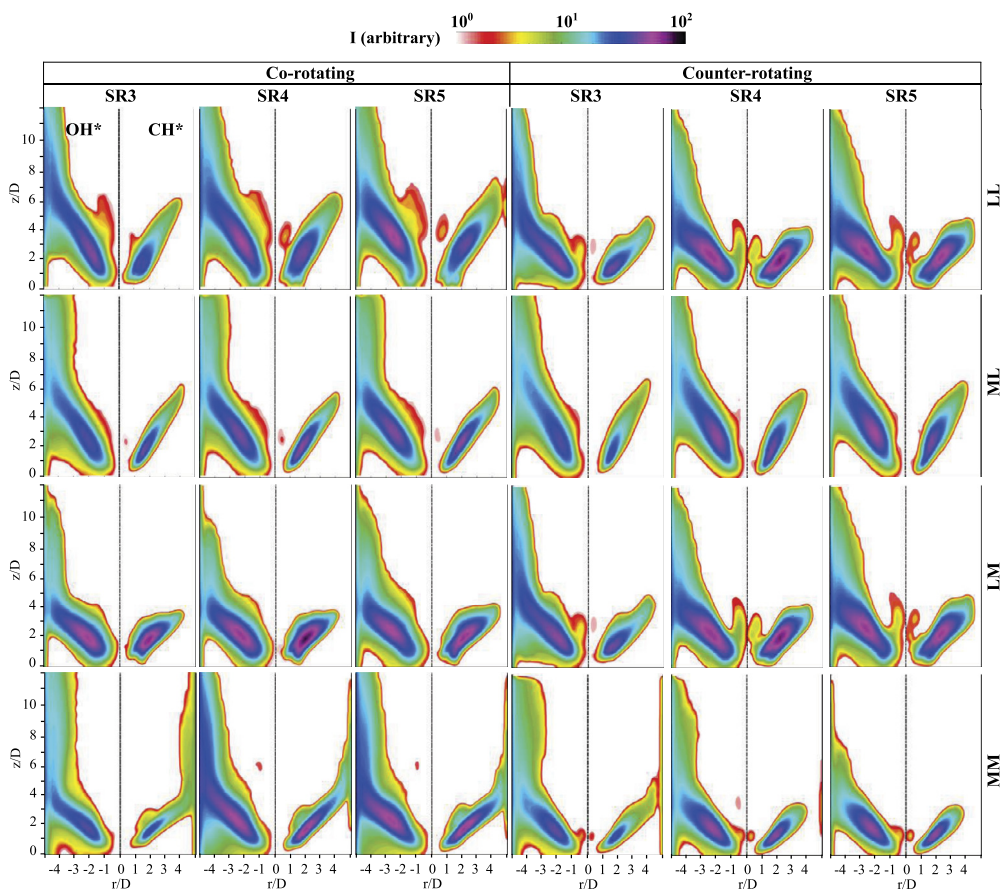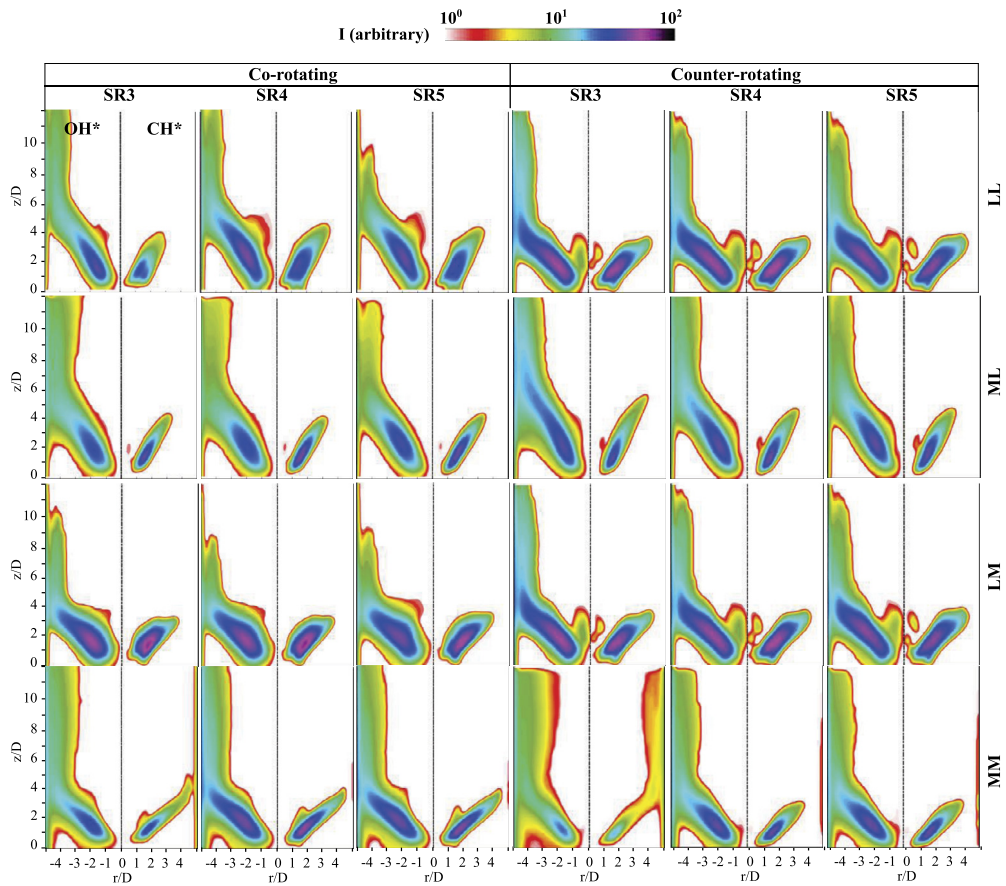
Fig. 12. Abel deconvoluted mean chemiluminescence intensity of OH* (r/D<0) and CH* (r/D>0) at various stratification levels for VR3 with co-rotating and counter rotating swirler combinations.
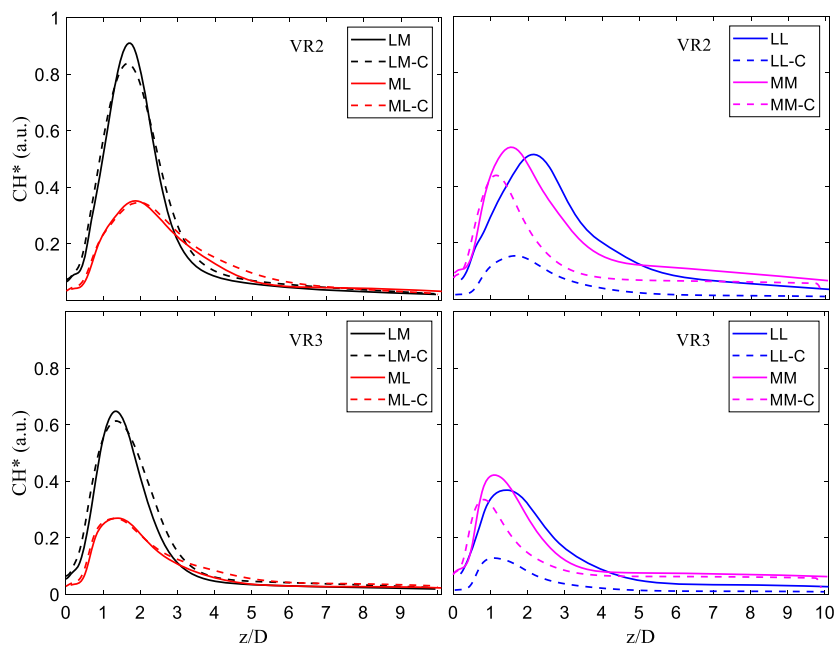

Fig. 13. Cumulative CH* intensity profiles along the axial direction for stratified flames (SR4) with various swirl configurations and velocity ratios.

support. When the swirl number changes, the stratified flame structure changes, but it is less sensitive to swirl direction changes. Because of the increased flame speed, highly stratified flames are more compact. As a result, the flame has less interaction with the quartz tube wall, resulting in less heat transfer to the wall.

Declaration of competing interest

The authors declare that they have no known competing financial interests or personal relationships that could have appeared to influence the work reported in this paper.

Acknowledgement

Appendix A. Supplementary material

Supplementary material related to this article can be found online at https://doi.org/10.1016/j.ast.2021.107253.

References

[1] H.S. Kim, V.K. Arghode, A.K. Gupta, Flame characteristics of hydrogen-enriched methane–air premixed swirling flames, Int. J. Hydrog. Energy 34 (2009) 1063–1073, https://doi.org/10.1016/j.ijhydene.2008.10.035.

[2] Y. Sun, M. Sun, J. Zhu, D. Zhao, Q. Wang, M. Wan, Y. Chen, Z. Cai, Y. Sun, Plif measurements of instantaneous flame structures and curvature of an acoustically excited turbulent premixed flame, Aerosp. Sci. Technol. 104 (2020) 105950, https://doi.org/10.1016/j.ast.2020.105950.

[3] Y. Cai, T. Li, M. Du, J. Li, Effects of thermodiffusive instability on the spherical premixed flames anchored to a porous-plug burner, Aerosp. Sci. Technol. 97 (2020) 105632, https://doi.org/10.1016/j.ast.2019.105632.

[4] H. Zhou, C. Tao, Z. Liu, S. Meng, K. Cen, Optimal control of turbulent premixed combustion instability with annular micropore air jets, Aerosp. Sci. Technol. 98 (2020) 105650, https://doi.org/10.1016/j.ast.2019.105650.

[5] Z. Rao, R. Li, B. Zhang, B. Wang, D. Zhao, M.S. Akhtar, Experimental investigations of equivalence ratio effect on nonlinear dynamics features in premixed swirl-stabilized combustor, Aerosp. Sci. Technol. 112 (2021) 106601, https://doi.org/10.1016/j.ast.2021.106601.

[6] C. Tao, H. Zhou, Dilution effects of co2, ar, n2 and he microjets on the combustion dynamic and emission characteristics of unsteady premixed flame, Aerosp. Sci. Technol. 111 (2021) 106537, https://doi.org/10.1016/j.ast.2021.106537.

[7] B. Böhm, J.H. Frank, A. Dreizler, Temperature and mixing field measurements in stratified lean premixed turbulent flames, Proc. Combust. Inst. 33 (2011) 1583–1590, https://doi.org/10.1016/j.proci.2010.06.139.

[8] S. Balusamy, A. Cessou, B. Lecordier, Laminar propagation of lean premixed flames ignited in stratified mixture, Combust. Flame 161 (2014) 427–437, https://doi.org/10.1016/j.combustflame.2013.08.023.

[9] G. Paterakis, E. Politi, P. Koutmos, Experimental investigation of isothermal scalar mixing fields downstream of axisymmetric baffles under fully premixed or stratified inlet mixture conditions, Exp. Therm. Fluid Sci. 108 (2019) 1–15, https://doi.org/10.1016/j.expthermflusci.2019.05.018.

[10] M. Sweeney, S. Hochgreb, M. Dunn, R. Barlow, The structure of turbulent stratified and premixed methane/air flames i: non-swirling flows, Combust. Flame 159 (2012) 2896–2911, https://doi.org/10.1016/j.combustflame.2012.06.001.

[11] M. Sweeney, S. Hochgreb, M. Dunn, R. Barlow, The structure of turbulent stratified and premixed methane/air flames ii: swirling flows, Combust. Flame 159 (2012) 2912–2929, https://doi.org/10.1016/j.combustflame.2012.05.014.

[12] R. Zhou, S. Balusamy, M.S. Sweeney, R.S. Barlow, S. Hochgreb, Flow field measurements of a series of turbulent premixed and stratified methane/air flames, Combust. Flame 160 (2013) 2017–2028, https://doi.org/10.1016/j.combustflame.2013.04.007.

[13] M.M. Kamal, R.S. Barlow, S. Hochgreb, Conditional analysis of turbulent premixed and stratified flames on local equivalence ratio and progress of reaction, Combust. Flame 162 (2015) 3896–3913, https://doi.org/10.1016/j.combustflame.2015.07.026.

[14] Y. Zhou, C. Zhang, X. Han, Y. Lin, Monitoring combustion instabilities of stratified swirl flames by feature extractions of time-averaged flame images using deep learning method, Aerosp. Sci. Technol. 109 (2021) 106443, https://doi.org/10.1016/j.ast.2020.106443.

[15] D. Sellan, S. Balusamy, Experimental study of swirl-stabilized turbulent premixed and stratified lpg/air flames using optical diagnostics, Exp. Therm. Fluid Sci. 121 (2021) 110281, https://doi.org/10.1016/j.expthermflusci.2020.110281.

[16] T. Kang, D.C. Kyritsis, Departure from quasi-homogeneity during laminar flame propagation in lean, compositionally stratified methane-air mixtures, Proc. Combust. Inst. 31 (2007) 1075–1083, https://doi.org/10.1016/j.proci.2006.07.051.

[17] V. Robin, A. Mura, M. Champion, O. Degardin, B. Renou, M. Boukhalfa, Experimental and numerical analysis of stratified turbulent v-shaped flames, Combust. Flame 153 (2008) 288–315, https://doi.org/10.1016/j.combustflame.2007.10.008.

[18] P. Anselmo-Filho, S. Hochgreb, R. Barlow, R. Cant, Experimental measurements of geometric properties of turbulent stratified flames, Proc. Combust. Inst. 32 (2009) 1763–1770, https://doi.org/10.1016/j.proci.2008.05.085.

[19] N. Pasquier, B. Lecordier, M. Trinité, A. Cessou, An experimental investigation of flame propagation through a turbulent stratified mixture, Proc. Combust. Inst. 31 (2007) 1567–1574, https://doi.org/10.1016/j.proci.2006.07.118.

[20] M.S. Sweeney, Measurements of the structure of turbulent premixed and stratified methane/air flames, Ph.D. thesis, Magdalene College, University of Cambridge, 2011.

[21] A.R. Masri, Partial premixing and stratification in turbulent flames, Proc. Combust. Inst. 35 (2015) 1115–1136, https://doi.org/10.1016/j.proci.2014.08.032.

[22] A. Pires Da Cruz, A. Dean, J. Grenda, A numerical study of the laminar flame speed of stratified methane/air flames, Symp., Int., Combust. 28 (2000) 1925–1932, https://doi.org/10.1016/S0082-0784(00)80597-4.

[23] E.S. Richardson, V.E. Granet, A. Eyssartier, J.H. Chen, Effects of equivalence ratio variation on lean, stratified methane-air laminar counterflow flames, Combust. Theory Model. 14 (2010) 775–792, https://doi.org/10.1080/13647830.2010.490881.

[24] P. Vena, B. Deschamps, G. Smallwood, M. Johnson, Equivalence ratio gradient effects on flame front topology in a stratified iso-octane/air turbulent v-flame, Proc. Combust. Inst. 33 (2011) 1551–1558, https://doi.org/10.1016/j.proci.2010.06.041.

[25] C. Karagiannaki, G. Paterakis, K. Souflas, E. Dogkas, P. Koutmos, Performance evaluation of a model swirl burner under premixed or stratified inlet mixture conditions, J. Energy Eng. 141 (2014) C4014010, https://doi.org/10.1061/(ASCE)EY.1943-7897.0000242.

[26] A.N. Lipatnikov, Stratified turbulent flames: recent advances in understanding the influence of mixture inhomogeneities on premixed combustion and modeling challenges, Prog. Energy Combust. Sci. 62 (2017) 87–132, https://doi.org/10.1016/j.pecs.2017.05.001.

[27] S. Barakat, H. Wang, T. Jin, W. Tao, G. Wang, Isothermal swirling flow characteristics and pressure drop analysis of a novel double swirl burner, AIP Adv. 11 (3) (2021) 035240.

[28] B. Dally, D. Fletcher, A. Masri, Flow and mixing fields of turbulent bluff-body jets and flames, Combust. Theory Model. 2 (1998) 193–219, https://doi.org/10.1088/1364-7830/2/2/006.

[29] Z. Mansouri, T. Boushaki, Experimental and numerical investigation of turbulent isothermal and reacting flows in a non-premixed swirl burner, Int. J. Heat Fluid Flow 72 (2018) 200–213, https://doi.org/10.1016/j.ijheatfluidflow.2018.06.007.

[30] E. Dogkas, E.P. Mitsopoulos, P. Koutmos, Mixing and combustion performance of a stratified bluff body primary zone interacting with a coannular swirl-induced recirculation, J. Energy Eng. 144 (4) (2018) 04018035, https://doi.org/10.1061/(ASCE)EY.1943-7897.0000551.

[31] S. Archer, A. Gupta, Effect of swirl on flow dynamics in unconfined and confined gaseous fuel flames, in: 42nd AIAA Aerospace Sciences Meeting and Exhibit, 2004, p. 813.

[32] C.T. Chong, S.S. Lam, S. Hochgreb, Effect of mixture flow stratification on premixed flame structure and emissions under counter-rotating swirl burner configuration, Appl. Therm. Eng. 105 (2016) 905–912, https://doi.org/10.1016/j.applthermaleng.2016.03.164.

[33] A. Degeneve, R. Vicquelin, C. Mirat, J. Caudal, T. Schuller, Impact of co- and counter-swirl on flow recirculation and liftoff of non-premixed oxy-flames above coaxial injectors, Proc. Combust. Inst. 38 (4) (2021) 5501–5508, https://doi.org/10.1016/j.proci.2020.06.279.

[34] D.S. Dandy, S.R. Vosen, Numerical and experimental studies of hydroxyl radical chemiluminescence in methane-air flames, Combust. Sci. Technol. 82 (1–6) (1992) 131–150, https://doi.org/10.1080/00102209208951816.

[35] Y. Hardalupas, M. Orain, Local measurements of the time-dependent heat release rate and equivalence ratio using chemiluminescent emission from a flame, Combust. Flame 139 (3) (2004) 188–207, https://doi.org/10.1016/j.combustflame.2004.08.003.

[36] Y. Ikeda, J. Kojima, T. Nakajima, F. Akamatsu, M. Katsuki, Measurement of the local flamefront structure of turbulent premixed flames by local chemiluminescence, Proc. Combust. Inst. 28 (1) (2000) 343–350, https://doi.org/10.1016/S0082-0784(00)80229-5.

[37] C. Lawn, W. Polifke, A model for the thermoacoustic response of a premixed swirl burner, part ii: the flame response, Combust. Sci. Technol. 176 (8) (2004) 1359–1390, https://doi.org/10.1080/00102200490461623.

[38] M. Orain, Y. Hardalupas, Effect of fuel type on equivalence ratio measurements using chemiluminescence in premixed flames, C. R., Méc. 338 (5) (2010) 241–254, https://doi.org/10.1016/j.crme.2010.05.002.

[39] J. Ballester, R. Hernández, A. Sanz, A. Smolarz, J. Barroso, A. Pina, Chemiluminescence monitoring in premixed flames of natural gas and its blends with hydrogen, Proc. Combust. Inst. 32 (2) (2009) 2983–2991, https://doi.org/10.1016/j.proci.2008.07.029.

[40] M.G. De Giorgi, A. Sciolti, S. Campilongo, A. Ficarella, Image processing for the characterization of flame stability in a non-premixed liquid fuel burner near lean blowout, Aerosp. Sci. Technol. 49 (2016) 41–51, https://doi.org/10.1016/j.ast.2015.11.030.

[41] C. Karagiannaki, E. Dogkas, G. Paterakis, K. Souflas, E.Z. Psarakis, P. Vasiliou, P. Koutmos, A comparison of the characteristics of disk stabilized lean propane flames operated under premixed or stratified inlet mixture conditions, Exp. Therm. Fluid Sci. 59 (2014) 264–274, https://doi.org/10.1016/j.expthermflusci.2014.04.002.

[42] Z. Han, S. Balusamy, S. Hochgreb, Spatial analysis on forced heat release response of turbulent stratified flames, J. Eng. Gas Turbines Power 137 (6) (2015), https://doi.org/10.1115/1.4029056.

[43] M.M. Kamal, Two-line (ch*/co2*) chemiluminescence technique for equivalence ratio mapping in turbulent stratified flames, Energy 192 (2020) 116485, https://doi.org/10.1016/j.energy.2019.116485.

[44] C. Ruan, F. Chen, W. Cai, Y. Qian, L. Yu, X. Lu, Principles of non-intrusive diagnostic techniques and their applications for fundamental studies of combustion instabilities in gas turbine combustors: a brief review, Aerosp. Sci. Technol. 84 (2019) 585–603, https://doi.org/10.1016/j.ast.2018.10.002.

[45] T. Yu, C. Ruan, F. Chen, Q. Wang, W. Cai, X. Lu, Measurement of the 3d Rayleigh index field via time-resolved ch* computed tomography, Aerosp. Sci. Technol. 95 (2019) 105487, https://doi.org/10.1016/j.ast.2019.105487.

[46] H. Liu, J. Zhao, C. Shui, W. Cai, Reconstruction and analysis of non-premixed turbulent swirl flames based on khz-rate multi-angular endoscopic volumetric tomography, Aerosp. Sci. Technol. 91 (2019) 422–433, https://doi.org/10.1016/j.ast.2019.05.025.

[47] T.Y. Kim, Y. Lee, C. Kim, M. Shin, Effects of shape and surface roughness on icing and condensation characteristics of an injector in a liquid phase lpg injection system, Fuel 132 (2014) 82–92, https://doi.org/10.1016/j.fuel.2014.04.010.

[48] Z. Liu, L. Li, B. Deng, Cold start characteristics at low temperatures based on the first firing cycle in an lpg engine, Energy Convers. Manag. 48 (2) (2007) 395–404, https://doi.org/10.1016/j.enconman.2006.07.011.

[49] C. Gong, K. Huang, B. Deng, X. Liu, Catalyst light-off behavior of a spark-ignition lpg (liquefied petroleum gas) engine during cold start, Energy 36 (1) (2011) 53–59, https://doi.org/10.1016/j.energy.2010.11.026.

[50] S. Liao, D. Jiang, Q. Cheng, J. Gao, Z. Huang, Y. Hu, Correlations for laminar burning velocities of liquefied petroleum gas-air mixtures, Energy Convers. Manag. 46 (2005) 3175–3184, https://doi.org/10.1016/j.enconman.2005.03.020.

[51] A.M. Elbaz, H.A. Moneib, K.M. Shebil, W.L. Roberts, Low nox - lpg staged combustion double swirl flames, Renew. Energy 138 (2019) 303–315, https://doi.org/10.1016/j.renene.2019.01.070.

[52] F. Li, M. Du, L. Yang, Effect of fuel injection parameters on performance characteristics and emissions of a thermoacoustic system, Aerosp. Sci. Technol. (2021) 106512, https://doi.org/10.1016/j.ast.2021.106512.

[53] K. Kihm, F. Sun, N. Chigier, Laser Doppler velocimetry investigation of swirler flowfields, J. Propuls. Power 6 (1990) 364–374, https://doi.org/10.2514/3.25445.

[54] A. Yoshida, M. Narisawa, H. Tsuji, T. Hirose, Chemiluminescence emission of c2, ch and oh radicals from opposed jet burner flames, JSME Int. J. Ser. B Fluids Therm. Eng. 38 (1995) 222–229, https://doi.org/10.1299/JSMEB.38.222.

[55] I. Hurle, R. Price, T.M. Sugden, A. Thomas, Sound emission from open turbulent premixed flames, Proc. R. Soc. Lond. Ser. A, Math. Phys. Sci. 303 (1475) (1968) 409–427, https://doi.org/10.1098/rspa.1968.0058.

[56] A. Caldeira-Pires, Free radical imaging techniques applied to hydrocarbon flames diagnosis, J. Therm. Sci. 10 (2) (2001) 182–187, https://doi.org/10.1007/s11630-001-0063-0.

[57] C.J. Dasch, One-dimensional tomography: a comparison of Abel, onion-peeling, and filtered backprojection methods, Appl. Opt. 31 (8) (1992) 1146–1152, https://doi.org/10.1364/AO.31.001146.